Institute for Advanced Technology
The University of Texas at Austin

Accounting for the Penetration Entrance Effect

Y. Partom
Institute for Advanced Technology
The University of Texas at Austin

February 1994

IAT.R 0039

REPORT DOCUMENTATION PAGE

Form Approved
OMB NO. 0704-0188

1. AGENCY USE ONLY (Leave blank)	2. REPORT DATE	3. REPORT TYPE AND DATES COVERED
	February 1994	Technical Report

4. TITLE AND SUBTITLE

Accounting for the Penetration Entrance Effect

5. FUNDING NUMBERS

Contract # DAAA21-93-C-0101

6. AUTHOR(S)

Y. Partom

7. PERFORMING ORGANIZATION NAME(S) AND ADDRESS(ES)

Institute for Advanced Technology
The University of Texas at Austin
4030-2 W. Braker Lane, #200
Austin, TX 78759

8. PERFORMING ORGANIZATION REPORT NUMBER

IAT.R 0039

9. SPONSORING / MONITORING AGENCY NAME(S) AND ADDRESS(ES)

U.S. Army Research Laboratory
ATTN: AMSRL-WT-T
Aberdeen Proving Ground, MD 21005-5066

10. SPONSORING / MONITORING AGENCY REPORT NUMBER

11. SUPPLEMENTARY NOTES

The view, opinions and/or findings contained in this report are those of the author(s) and should not be considered as an official Department of the Army position, policy, or decision, unless so designated by other documentation.

12a. DISTRIBUTION / AVAILABILITY STATEMENT

Approved for public release; distribution unlimited.

12b. DISTRIBUTION CODE

A

13. ABSTRACT *(Maximum 200 words)*

By running simulations in which we constrained the backward motion of the entrance boundry, we show that the entrance effect is not caused by the boundary motion. We use a simple time dependent Tate model to show that the entrance effect is caused by the initial (1D strain) high penetration velocity, and by the time dependency of the penetration process.

14. SUBJECT TERMS

entrance effect, penetration, penetration velocity, Tate model

15. NUMBER OF PAGES

22

16. PRICE CODE

17. SECURITY CLASSIFICATION OF REPORT	18. SECURITY CLASSIFICATION OF THIS PAGE	19. SECURITY CLASSIFICATION OF ABSTRACT	20. LIMITATION OF ABSTRACT
Unclassified	Unclassified	Unclassified	UL

Accounting for the Penetration Entrance Effect

Yehuda Partom

Abstract

By running simulations in which we constrained the backward motion of the entrance boundary, we show that the entrance effect is not caused by the boundary motion. We use a simple time dependent Tate model to show that the entrance effect is caused by the initial (1D strain) high penetration velocity, and by the time dependency of the penetration process.

1. Introduction

Running a computer simulation of a long rod penetration event, one can see clearly an entrance boundary effect. Figures 1 and 2 are output plots from an AUTODYN/EULER run of a L/D = 10 tungsten alloy rod at V = 1.5 km/s into a RHA steel target. The figures are taken from our report about the projectile-flow effect [1]. The plots in Figures 1 and 2 are from a run with a strain softening projectile material according to:

$$Y = Y_o\left(1 - \beta\, \varepsilon^p_{eff}\right) \quad , \tag{1}$$

where: Y = flow stress, Y_o = yield stress = 2 GPa, ε^p_{eff} = effective plastic strain, and $\beta = 0.25$. We chose to show the results of this run because strain softening enhances the contrast between the entrance and the quasi steady state regimes.

We see that initially, penetration velocity is significantly higher than during the quasi steady state phase. Also, deceleration of the penetration velocity is higher up to $t \cong 25\ \mu s$ (penetration of about three diameters). This behavior is typical of long rod penetration events, and we refer to it as the "entrance effect." In contrast to what we get from a simulation, there is no entrance effect in a Tate model run.

In Figure 3, we show a penetration-erosion curve from a Tate run of the same problem, with Y_p = 2 GPa and R_t = 5 GPa. We see no entrance effect, and the end (secondary) phase also looks different.

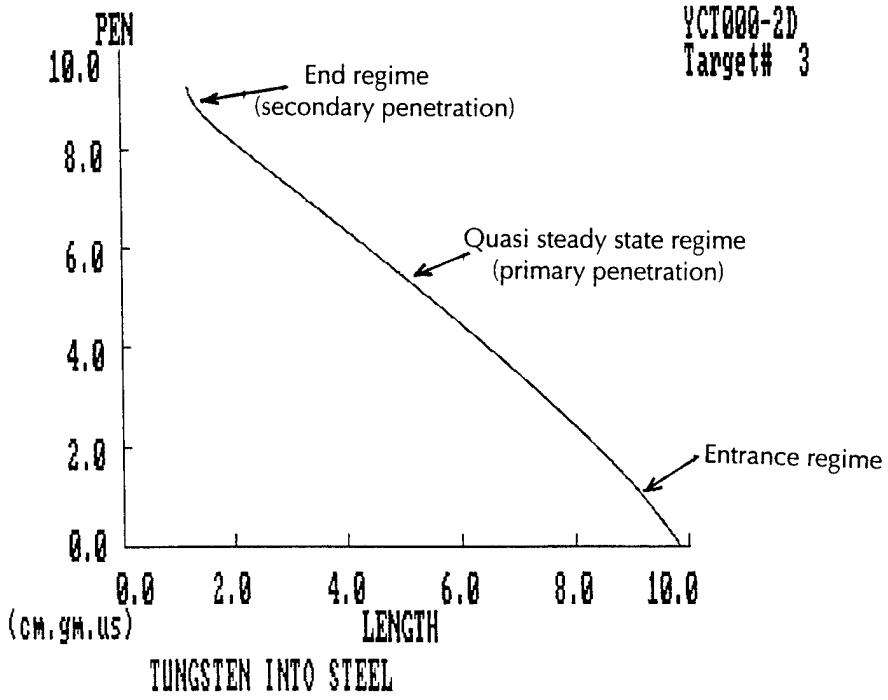

Figure 1. Penetration-erosion curve from an AUTODYN run of a L/D = 10 tungsten alloy rod penetrating RHA steel at 1.5 km/s.

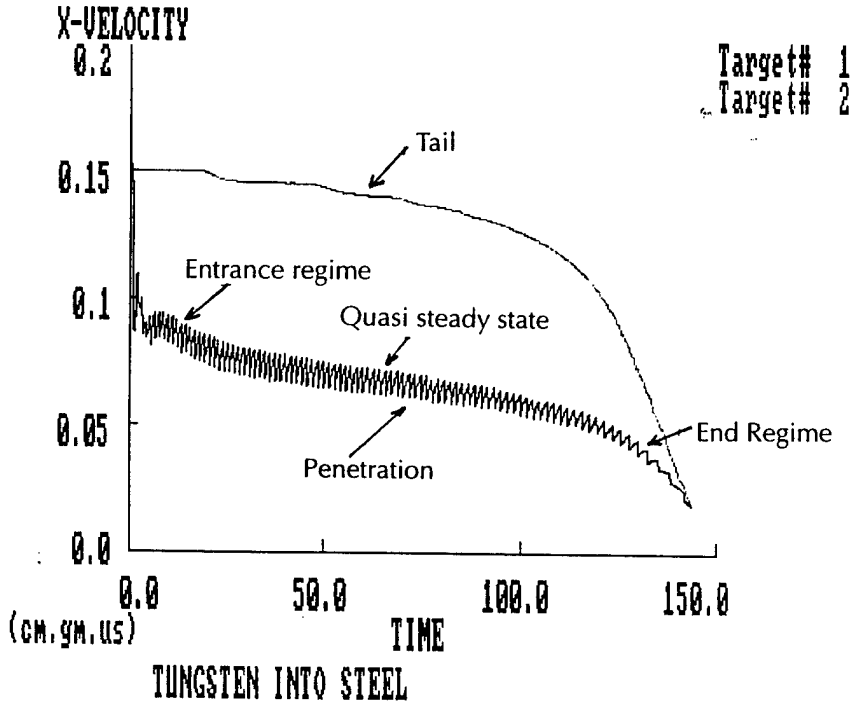

Figure 2. Penetration velocity and projectile tail velocity histories for the same run as in Figure 1.

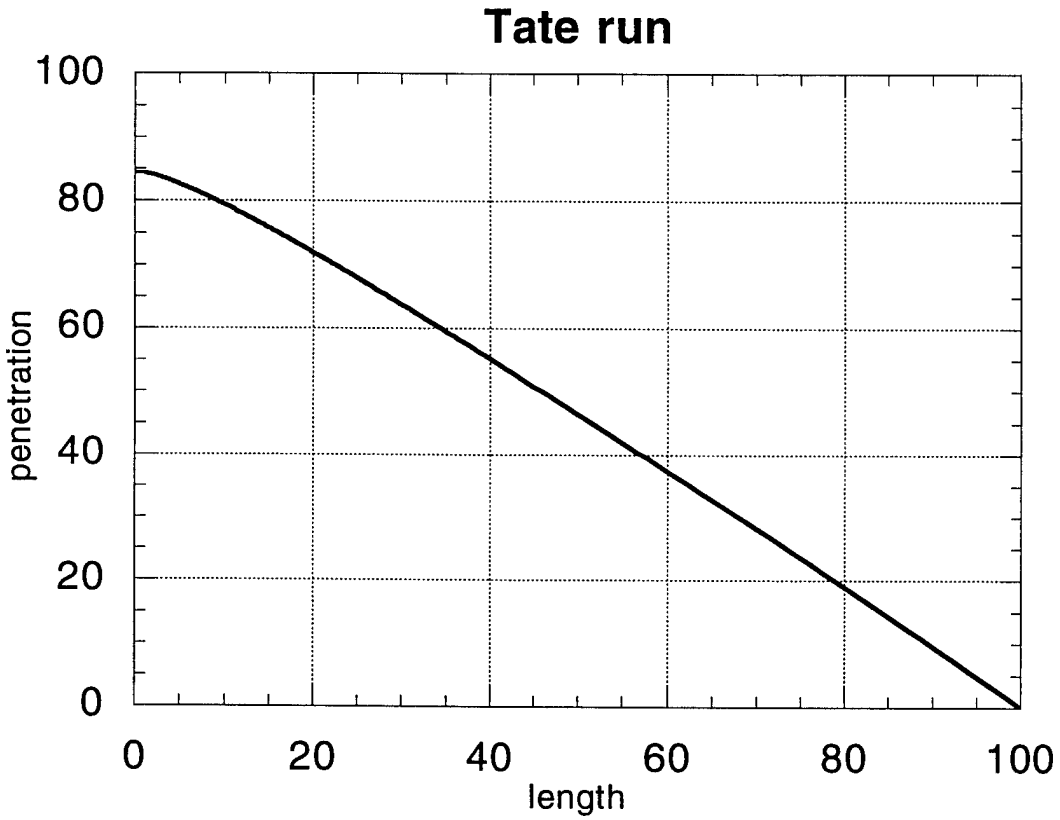

Figure 3. Penetration-erosion curve from a Tate run of a L = 100 mm tungsten alloy rod into RHA steel at 1.5 km/s. Y_p = 2 GPa, R_t = 5 GPa

In Figure 4, we show a typical plot from an AUTODYN simulation of material boundaries and velocity arrows at about 9 μs (~ ½D) into the penetration process. We see that a typical lip is formed on the target front surface around the crater. Because of this lip, and the backward target motion that creates it, we used to think that target resistance is lower near the entrance boundary, leading to the entrance effect. We used to advocate this "understanding" quite vigorously, and even devised a way to estimate the reduced resistance using a cavity expansion approach [2]. This view is not shared by other investigators [3] who claim that the entrance effect results from the initial shock phase and the high (1D strain) particle velocity associated with it.

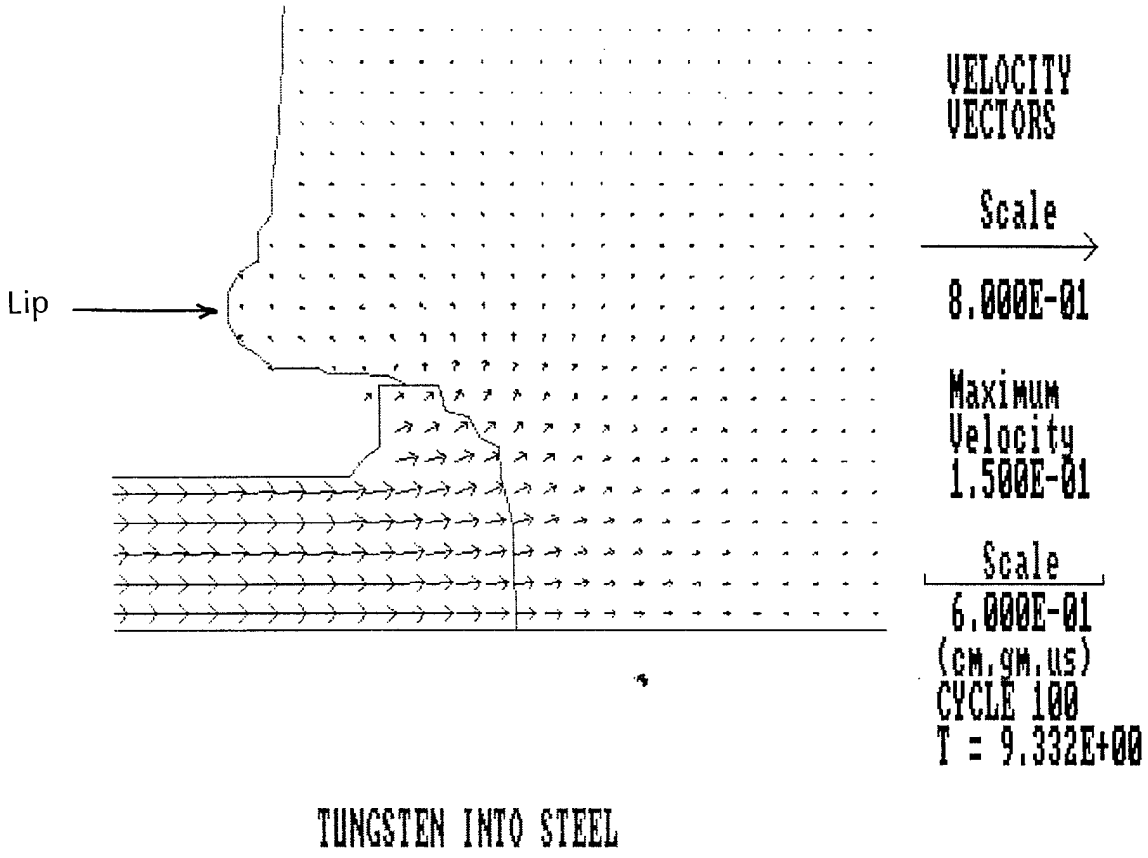

Figure 4. Material boundaries and velocity arrows plot from an AUTODYN simulation at about ½D penetration.

In what follows, we investigate the origin of the entrance effect by means of AUTODYN simulations. We do this by inhibiting the backward motion of a part of the entrance boundary. We find that the entrance effect is not affected by the inhibition of the backward motion of the entrance boundary.

Recently Walker and Anderson [4] proposed a time-dependent model for long rod penetration, so-called WA model. It is based on integration of the momentum equation along the projectile-target center line. Among other things, Walker and Anderson show that their model captures quite well the entrance effect.

In what follows, we use Walker and Anderson's approach to formulate what can be called a time dependent Tate model. It is a much simplified version of the WA model. Running this model, we show that it too is able to capture the entrance effect.

2. Simulations

We are using AUTODYN/EULER version 2.65. The tungsten alloy (projectile) and RHA steel (target) material models and parameters are the same as in [1] and [5]. The projectile radius is D/2 = 5 mm, and the Euler cell size is 1 x 1 mm so that there are five cells across the radius. This may not be enough to obtain convergent results, as shown in [6]. But as our purpose is to investigate the origin of the entrance effect (and not to compare simulations to experiments), five cells across the radius seem satisfactory. The projectile aspect ratio is L/D = 10, and the impact velocity V = 1.5 km/s.

We terminated our runs after 400 cycles (approximately 40 μs) and plotted material status plots every 100 cycles.

In all runs the entrance boundary is stress free on a ring $D/2 < r \leq D/2 + \Delta r$, and constrained in the axial direction elsewhere ($r > D/2 + \Delta r$). The different runs are listed in Table 1.

Table 1

List of Simulation Runs

No.	Δr mm
1	1
2	2
3	5
4	10
5	∞

Results for a regular run (unconstrained boundary, run no. 5) are shown in Figures 5 and 6). In Figure 5, we show material status plots at 100, 200, 300, and 400 cycles. In Figure 6, we show velocity vectors near the interface at the same times.

Figure 7 shows material status plots at cycle 300 for runs 1 to 4, and in Figure 8, the corresponding velocity vectors plots. We see that when Δr = 1 and 2 mm, the target material is not able to flow through the gap. For Δr = 5 and 10 mm, target material flows through the gap and a lip is formed. But in all cases, the penetration is the same, and the mushroom configuration is the same. The amount of backwards flow of the target boundary does not seem to influence the penetration process.

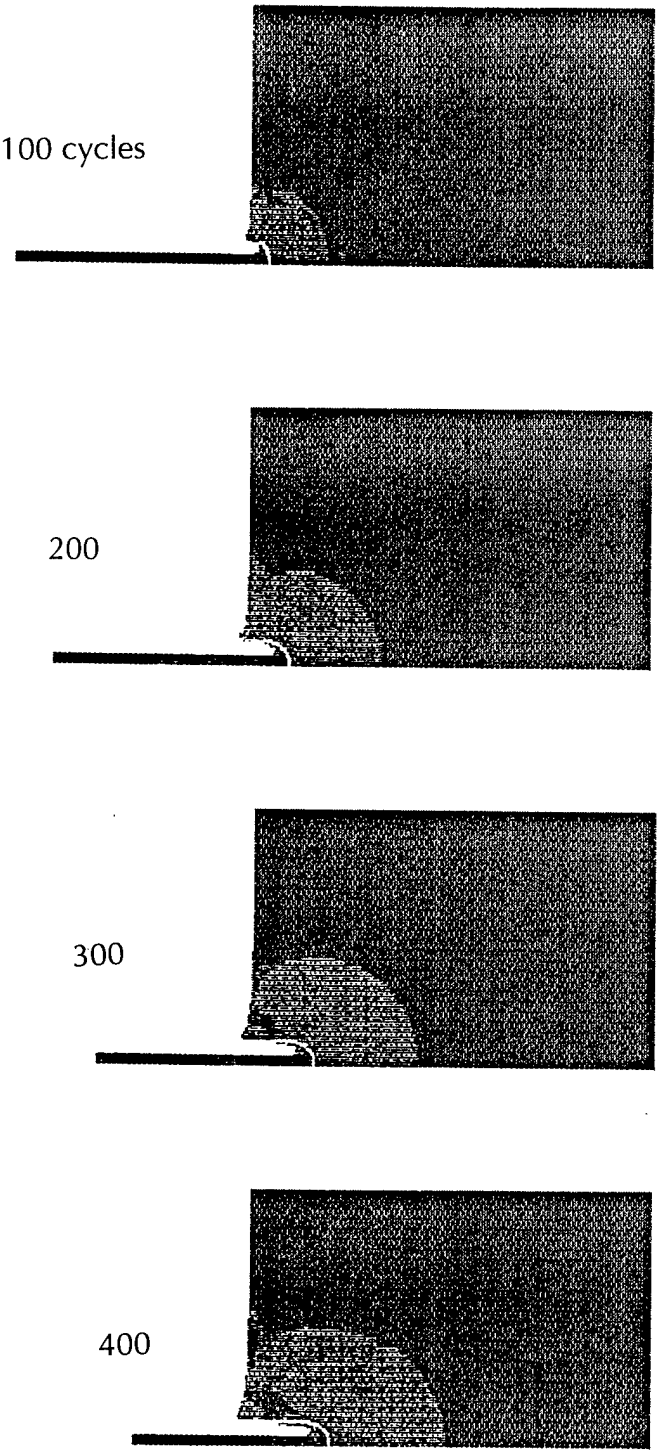

Figure 5. Material status plots for a regular run (no. 5).

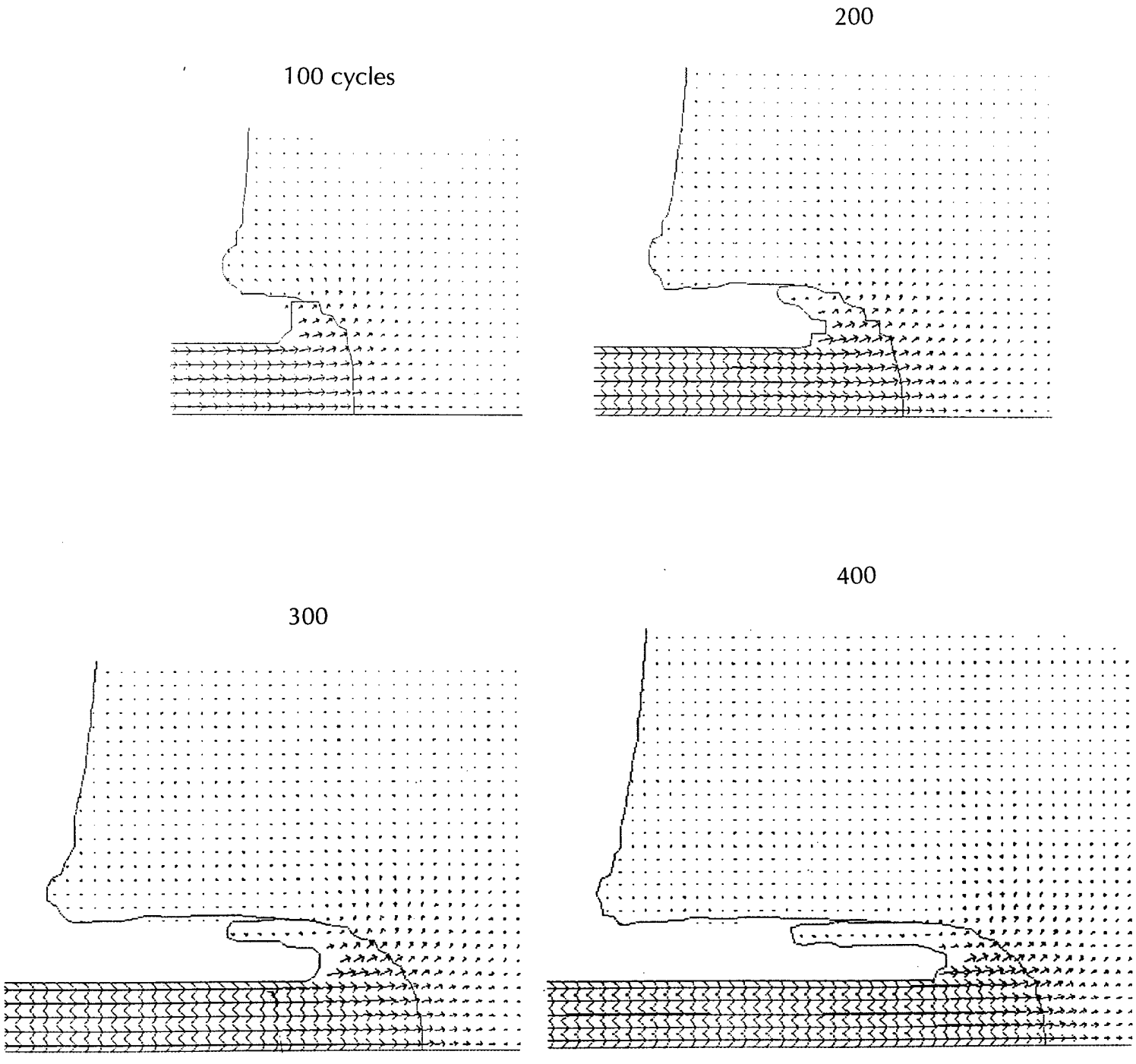

Figure 6. Velocity vectors plots for a regular run (no. 5).

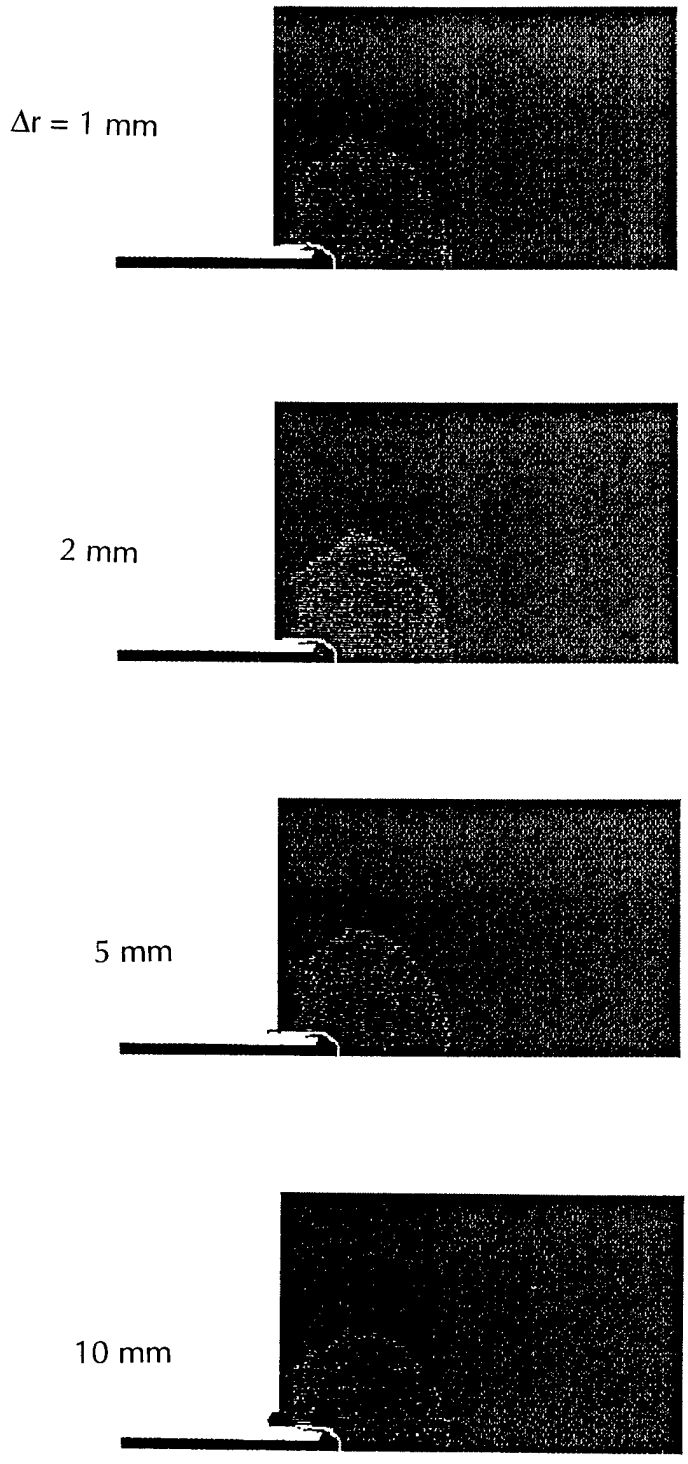

Figure 7. Material status plots at 300 cycles for runs 1 to 4.

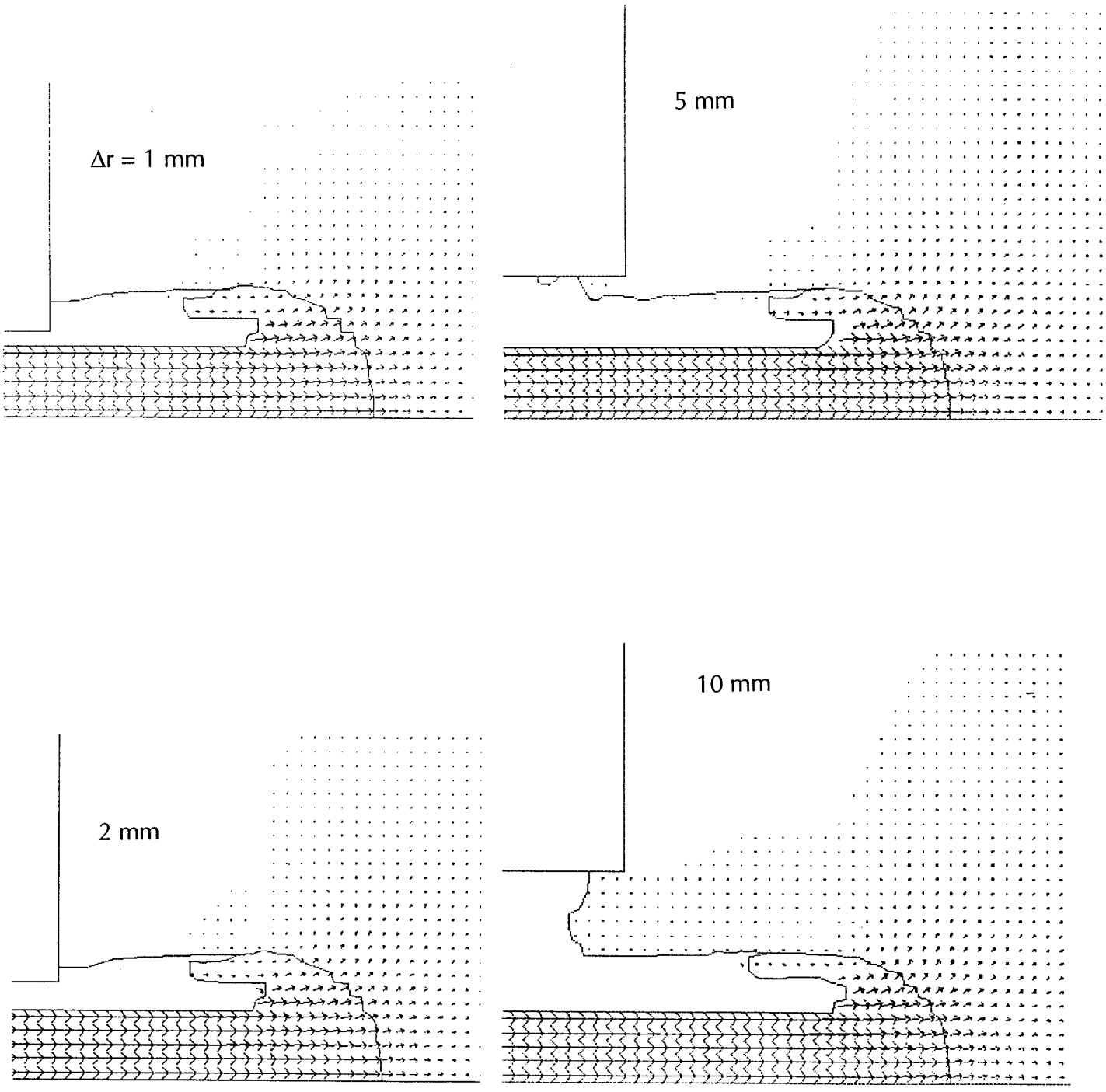

Figure 8. Velocity vectors plots at 300 cycles for runs 1 to 4.

To see this even more clearly, we show penetration velocity histories and penetration-erosion curves for runs 1 and 5 in Figures 9 and 10 . From Figure 9, we can see that the penetration velocity histories are practically the same. From Figure 10, we can see that the penetration-erosion curves are also practically the same, and that they both show the entrance effect.

We conclude from the simulations that the entrance effect is not caused by low target resistance near the entrance boundary.

In the next section we propose, as did Walker and Anderson [4], that the entrance effect can be accounted for by time dependency of the penetration process.

3. Time Dependent Tate Model

Walker and Anderson [4] have shown that by integrating the axial momentum equation along the projectile-target center line, one gets the following relation:

$$\rho_p \int_{x_p}^{x_i} \frac{\partial u}{\partial t} dx + \rho_t \int_{x_i}^{x_t} \frac{\partial u}{\partial t} dx + \frac{1}{2} \rho_p \left\langle [u(x_i)]^2 - [u(x_p)]^2 \right\rangle + \frac{1}{2} \rho_t \left\langle [u(x_t)]^2 - [u(x_i)]^2 \right\rangle$$

$$- \left[\sigma_{xx}(x_t) - \sigma_{xx}(x_p)\right] - 2 \int_{x_p}^{x_i} \frac{\partial \sigma_{xy}}{\partial y} dx - 2 \int_{x_i}^{x_t} \frac{\partial \sigma_{xy}}{\partial y} dx = 0 \qquad (2)$$

where:

x = axial direction, y = transverse direction, u = axial particle velocity, t = time, σ_{ij} = cartezian stress components, ρ_p = projectile density (assumed constant), ρ_t = target density (assumed constant), $x_p \le x \le x_t$ is the integration range along the center line (y = 0).

Unlike Walker and Anderson, we choose (in what follows) x_p to be the elastic-plastic boundary in the projectile, and x_t the elastic-plastic boundary in the target. x_i is the projectile-target interface.

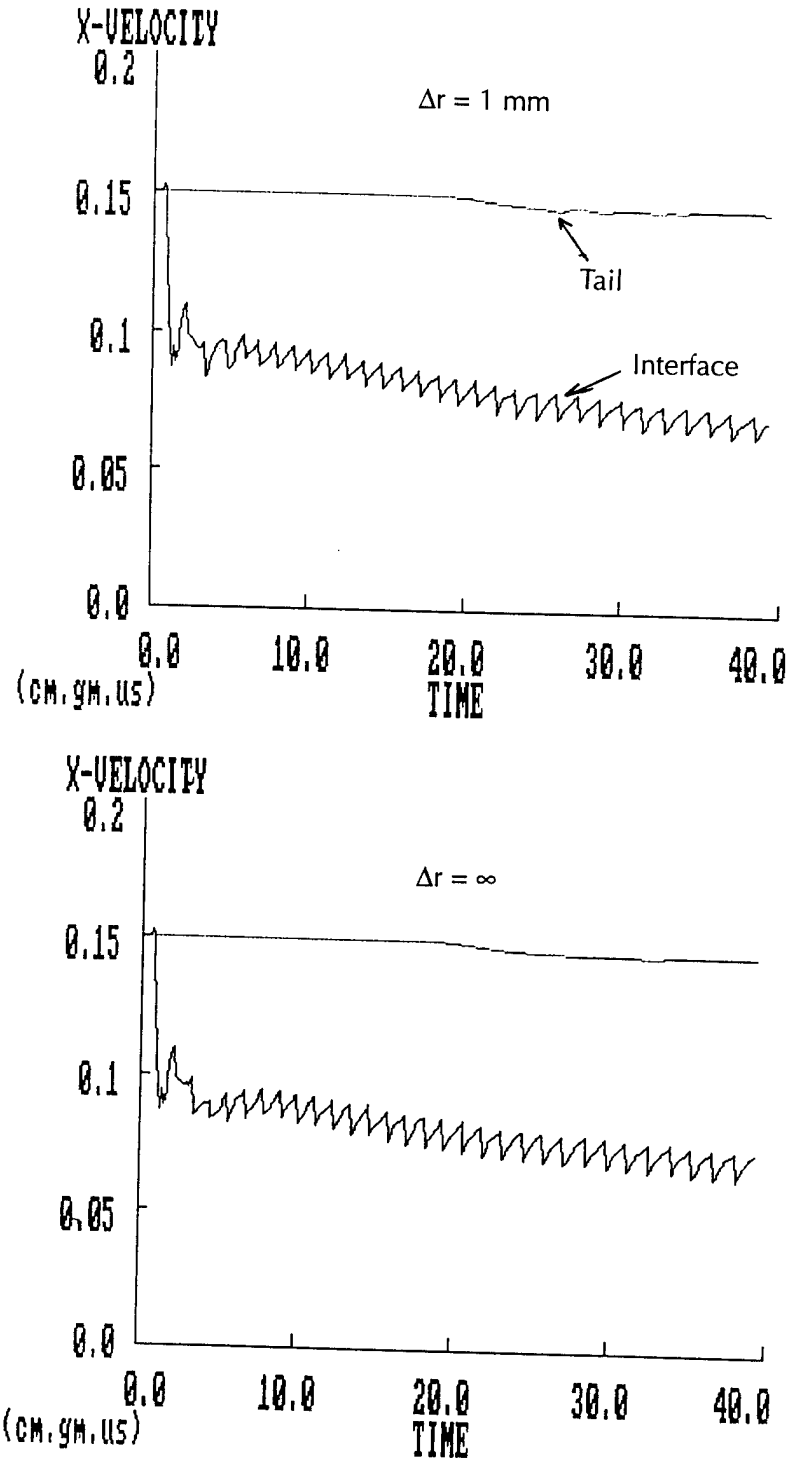

Figure 9. Penetration velocity and projectile tail velocity histories for runs 1 and 5.

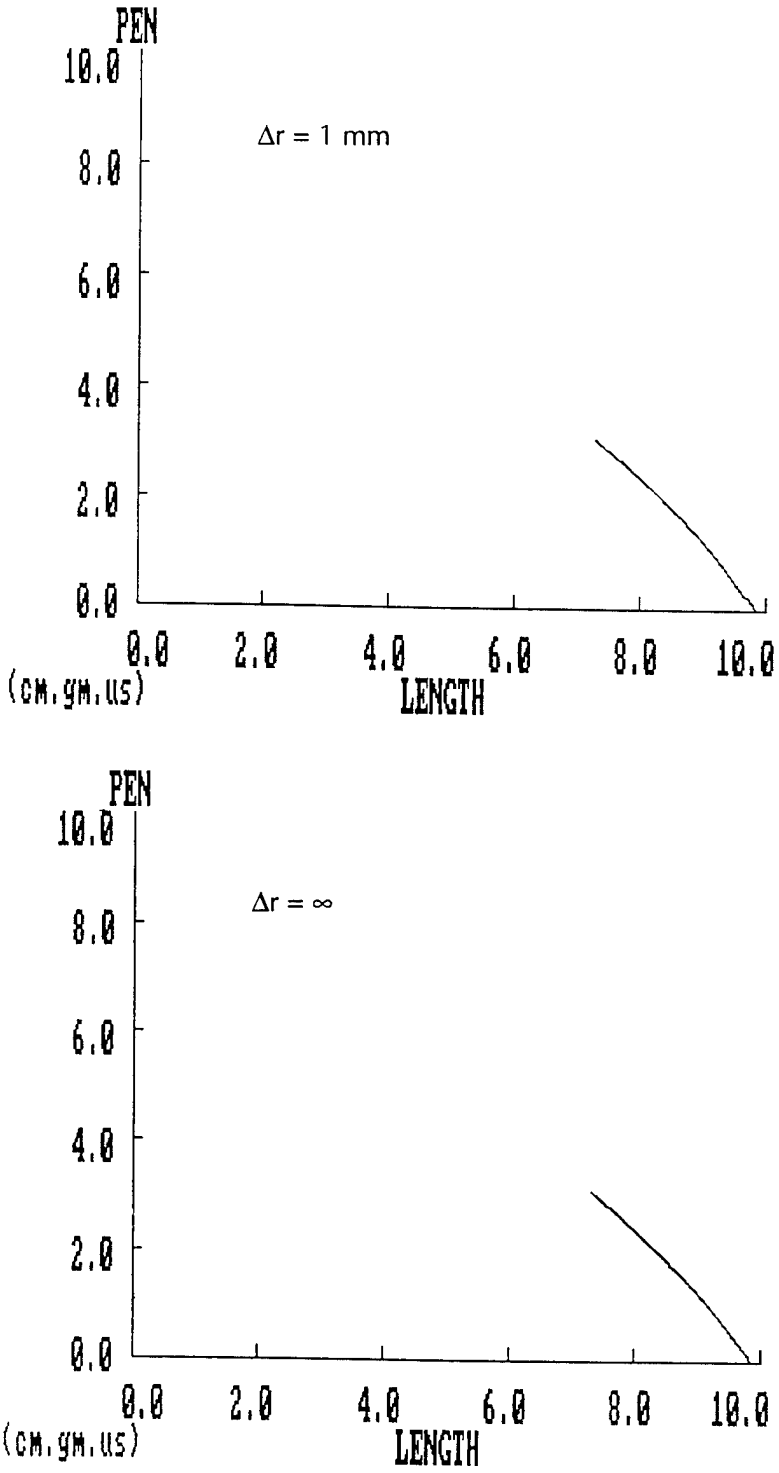

Figure 10. Penetration-erosion curves for runs 1 and 5.

In what follows, we use:

$$u(x_p) = V \text{ (projectile tail velocity)} , \tag{3}$$

$$u(x_i) = U \text{ (penetration velocity)} , \tag{4}$$

and assume:

$$u(x_t) \cong 0 . \tag{5}$$

Walker and Anderson went on to evaluate the last two integrals in Eq. (2) by assuming a specific form for the flow field u(x, y). We are using a simpler approach. Recognizing, as did Walker and Anderson, that:

$$- \sigma_{xx}(x_t) - 2 \int_{x_i}^{x_t} \frac{\partial \sigma_{xy}}{\partial y} dx = R_t \tag{6}$$

$$\sigma_{xx}(x_p) - 2 \int_{x_p}^{x_i} \frac{\partial \sigma_{xy}}{\partial y} dx = Y_p , \tag{7}$$

where R_t and Y_p are the Tate model target resistance and projectile strength, respectively.

We get from Eq. (2):

$$\rho_t \int_{x_i}^{x_t} \frac{\partial u}{\partial t} dx - \frac{1}{2} \rho_t U^2 + R_t = -\rho_p \int_{x_p}^{x_i} \frac{\partial u}{\partial t} dx - \frac{1}{2} \rho_p (U^2 - V^2) + Y_p \tag{8}$$

To evaluate the integrals in Eq. (8), we make the following simplifying assumptions:

$$x_i - x_p = \text{const.} = S_p , \tag{9}$$

$$x_t - x_i = \text{const.} = S_t\,, \tag{10}$$

$$u = U + (V-U)\, f_p\,(x) \qquad \text{in the projectile,} \tag{11}$$

and

$$u = U f_t\,(x) \qquad \text{in the target,} \tag{12}$$

where the functions f_p and f_t are advected without change at a velocity U, as shown in Figure 11.

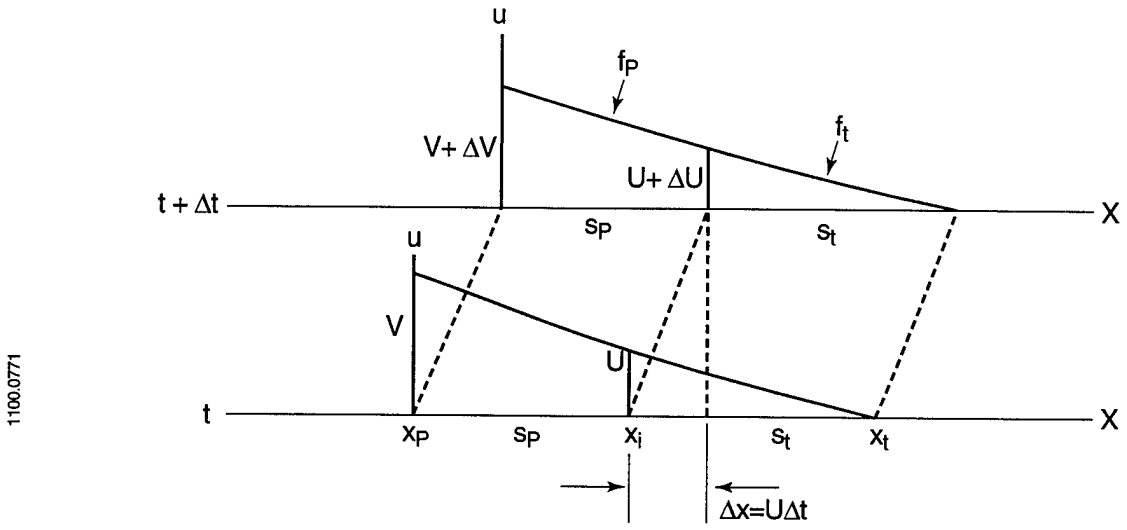

Figure 11. Simplified flow field on center line.

The advection assumption leads to:

$$\frac{\partial f_p}{\partial t} = - U \frac{\partial f_p}{\partial x} \tag{13}$$

$$\frac{\partial f_t}{\partial t} = - U \frac{\partial f_t}{\partial x} \tag{14}$$

so that in the projectile:

$$\frac{\partial u}{\partial t} = \frac{dU}{dt} + \left(\frac{dV}{dt} - \frac{dU}{dt}\right) f_p - U(V-U) \frac{\partial fp}{\partial x} \tag{15}$$

and in the target:

$$\frac{\partial u}{\partial t} = \frac{dU}{dt} f_t - U^2 \frac{\partial f_t}{\partial x} \quad . \tag{16}$$

Evaluating the integrals in Eq. (8) we get:

$$\int_{x_p}^{x_i} \frac{\partial u}{\partial t} dx = S_p \frac{dU}{dt} + \kappa_p S_p \left(\frac{dV}{dt} - \frac{dU}{dt}\right) + U(V-U) \tag{17}$$

$$\int_{x_i}^{x_t} \frac{\partial u}{\partial t} dx = \kappa_t S_t \frac{dU}{dt} + U^2 \tag{18}$$

where κ_p, κ_t are shape factors. For f_p, f_t linear, $\kappa_p = \kappa_t = 1/2$. For f_p, f_t concave 2nd degree parabolas, $\kappa_p = \kappa_t = 1/3$.

Substituting for the integrals from Eqs. (17) and (18) into Eq. (8) and rearranging, we finally get:

$$R_t + \frac{1}{2}\rho_t U^2 + \frac{dU}{dt}\left[\rho_p S_p (1 - \kappa_p) + \rho_t S_t \kappa_t\right] =$$

$$= Y_p + \frac{1}{2} \rho_p (V-U)^2 - \rho_p S_p \kappa_p \frac{dV}{dt} \tag{19}$$

We see that Eq. (19) collapses to Tate's equation (modified Bernouli equation) when $\frac{dU}{dt} = \frac{dV}{dt} = 0$ (steady-state assumption). We therefore refer to Eq. (19) as the "time dependent Tate equation." Using Eq. (19) together with the kinematic relations of Tate's model we thus define a time dependent Tate model, as follows:

$$\frac{dU}{dt} = F\left(U, V, \frac{dV}{dt}\right) \tag{20}$$

as defined by Eq. (19).

$$\frac{dV}{dt} = -\frac{Y_p}{\rho_p (L - S_p)} \tag{21}$$

$$\frac{dL}{dt} = -(V - U) \tag{22}$$

$$\frac{dp}{dt} = U \tag{23}$$

with the initial conditions:

$$V(0) = V_o \text{ (impact velocity)} \tag{24}$$

$$U(0) = U_o \text{ (1D strain interface velocity)} \tag{25}$$

$$L(0) = L_o \tag{26}$$

$$p(0) = 0 \tag{27}$$

We integrate the four ODEs Eqs. (20) to (23) using a standard ODE system solver.

At the end phase of the integration, $|dV/dt|$ becomes large as $L - S_p$ becomes small. Because of that, using Eq. (19) to evaluate dU/dt becomes unreliable. We therefore switch to a more robust way to compute dU/dt as follows:

We compute $\left(\frac{dU}{dt}\right)_{Tate}$ by:

$$\left(\frac{dU}{dt}\right)_{Tate} = \frac{\rho_p (V-U)}{\rho_t U + \rho_p (V-U)} \frac{dV}{dt} \qquad (28)$$

as obtained from differentiating Tate's equation and we get:

$$\left(-\frac{dU}{dt}\right) = \max\left[\left(-\frac{dU}{dt}\right)_{Eq.\ 19}, \left(-\frac{dU}{dt}\right)_{Tate}\right] \qquad (29)$$

To see how the time dependent Tate model performs, we compare it to the regular Tate model and to simulation results. The example we show is for an L/D = 10 tungsten alloy rod penetrating an RHA steel target. The model parameters are:

ρ_p = 17.3 g/cc, Y_p = 2 GPa, S_p = 14mm, κ_p = 0.5,

ρ_t = 7.85 g/cc, R_t = 6 GPa, S_t = 65 mm, κ_t = 0.3,

V_o = 1.5 km/s, U_o = 1 km/s, L_o = 100 mm.

In Figures 12.1 to 12.3, we show history plots from the simulation (U(t), p(t), and p(L)).

In Figures 13.1 to 13.3, we show the same history plots obtained from the time dependent Tate and from the regular Tate models. We copied on these plots the curves from Figures 12.1 to 12.3, respectively.

We see the following:

- The entrance effect is captured quite well by the time dependent Tate model.

- As expected, the time dependent Tate does not do well at the end phase.

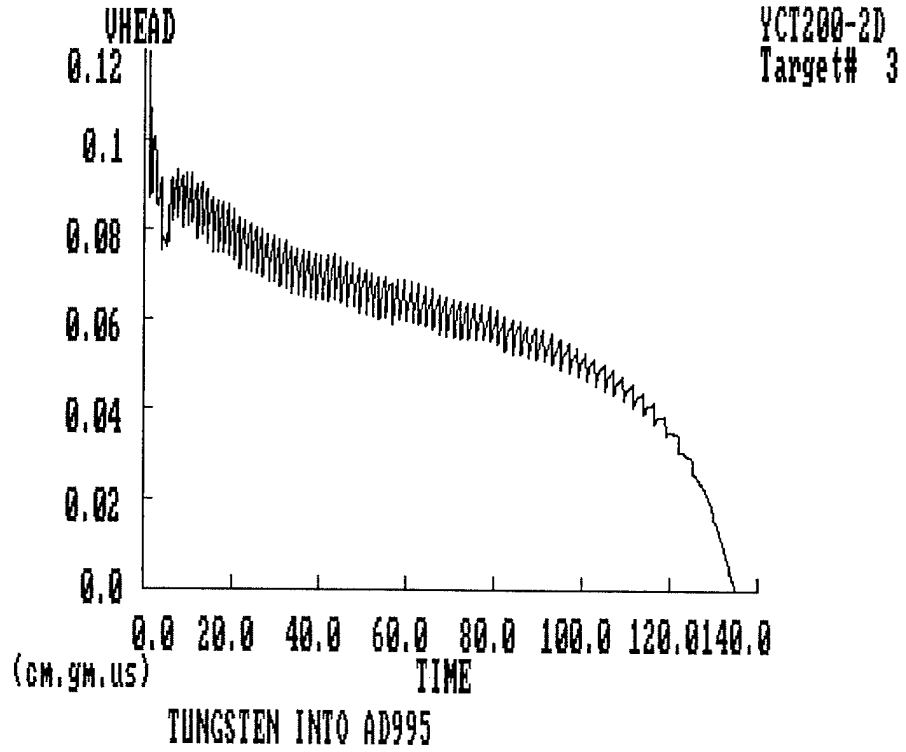

Figure 12.1. Penetration velocity history from the simulation.

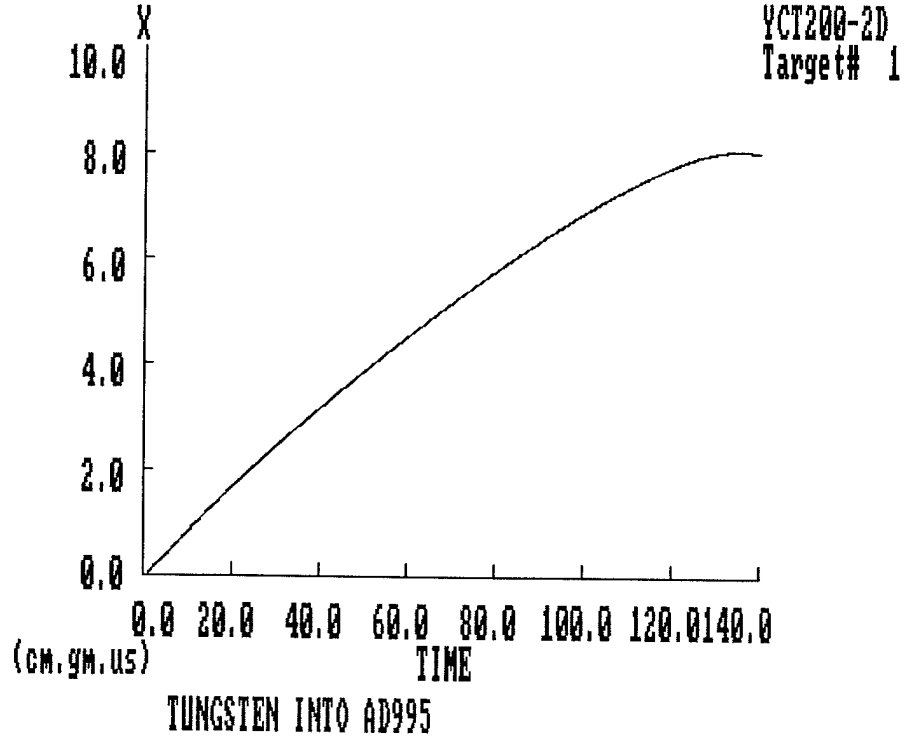

Figure 12.2. Penetration history from the simulation.

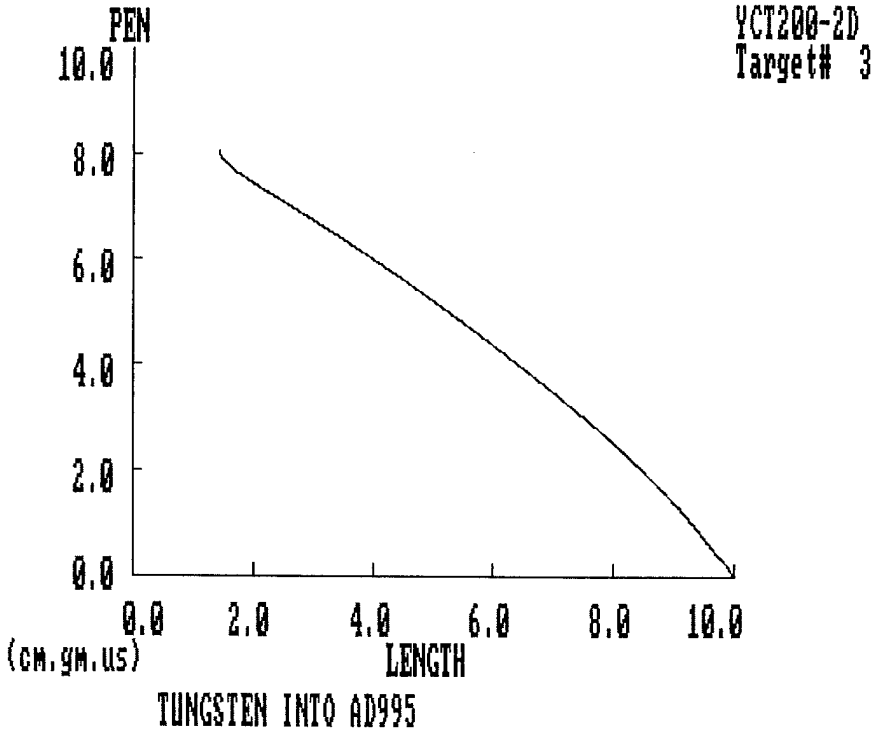

Figure 12.3. Penetration-erosion history from the simulation.

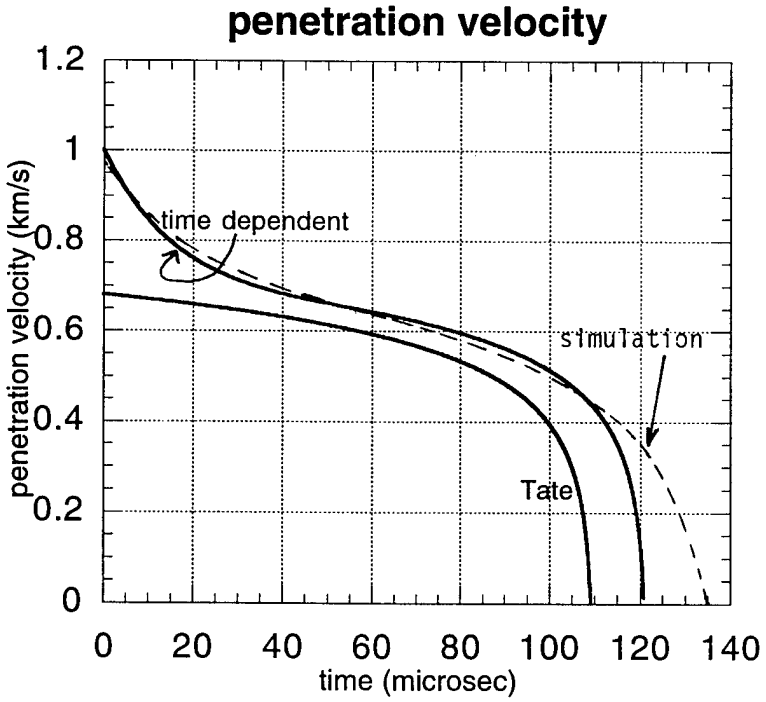

Figure 13.1. Penetration velocity histories.

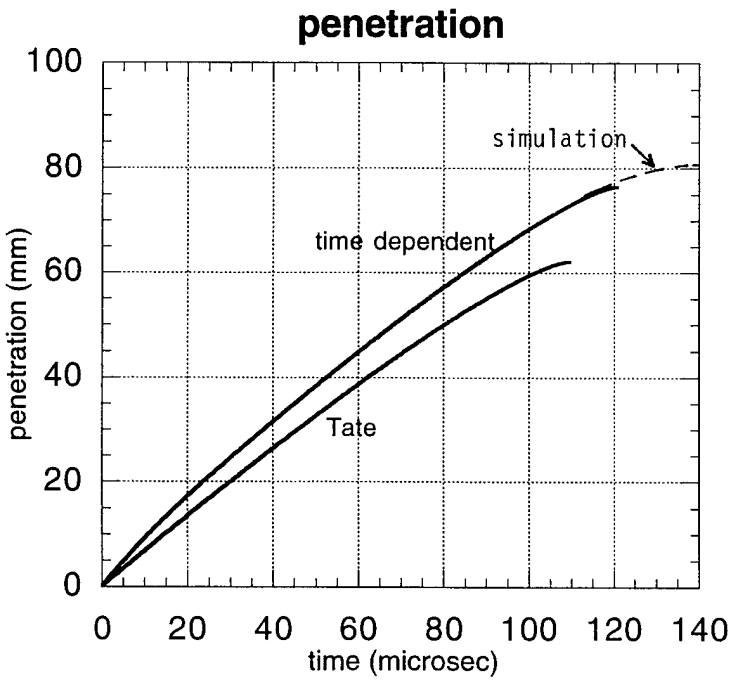

Figure 13.2. Penetration histories.

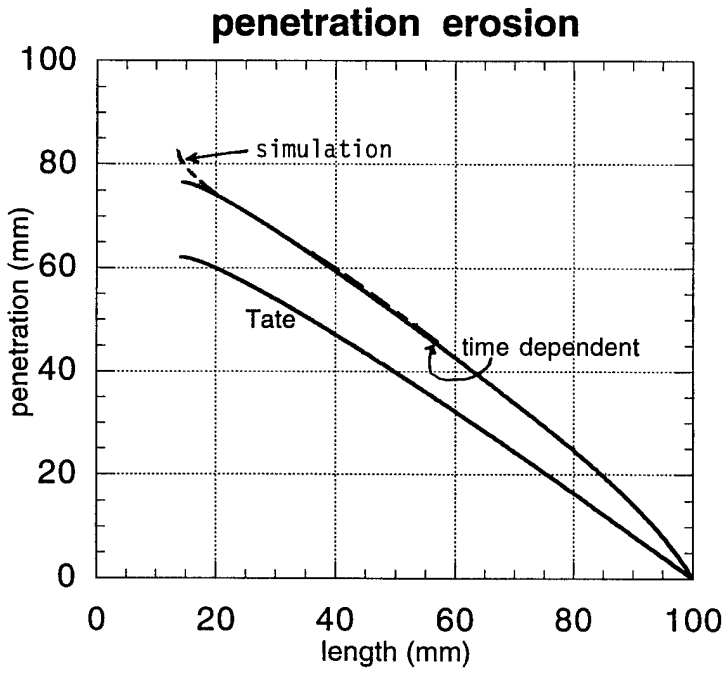

Figure 13.3. Penetration-erosion histories.

4. Conclusions

We ran computer simulations with AUTODYN to investigate the origin of the entrance effect in long rod penetration. By constraining the backward motion of the entrance boundary, we show that the entrance effect does not depend on the motion of the entrance boundary.

Based on Walker and Anderson's approach [4] of integrating the momentum equation along the axis, we propose a time dependent Tate model. Running the model and comparing to simulation results we show that the model captures quite well the entrance effect.

We conclude that the entrance effect results from the initial high (1D strain) penetration velocity, and from the time dependency of the penetration process.

Acknowledgments

This work was supported by the U.S. Army Armament Research, Development and Engineering Center (ARDEC) under contract DAAA21-90-D-0009.

References

[1] Yehuda Partom, "Projectile-Flow Effect for Long Rod Penetration," IAT.R 0036, February 1994.

[2] Yehuda Partom, "RAFAEL Internal Report (in Hebrew)," 1992.

[3] Charles E. Anderson, et al., private discussion, 1993.

[4] James D. Walker and Charles E. Anderson, "A Time-Dependent Model for Long-Rod Penetration," submitted to *Int. J. Impact Engng.*, 1993.

[5] Y. Partom, "Comparison of Penetration Efficiency in Axial and Planar Symmetries," IAT.R 0033, November 1993.

[6] Y. Partom and D. L. Littlefield, "Comparison of AUTODYN/EULER Penetration Runs to CTH," IAT.TN 0029, February 1994.

Distribution List

Administrator
Defense Technical Information Center
Attn: DTIC-DDA
8725 John J. Kingman Road, Ste 0944
Ft. Belvoir, VA 22060-6218

Director
US Army Research Lab
ATTN: AMSRL OP SD TA
2800 Powder Mill Road
Adelphi, MD 20783-1145

Director
US Army Research Lab
ATTN: AMSRL OP SD TL
2800 Powder Mill Road
Adelphi, MD 20783-1145

Director
US Army Research Lab
ATTN: AMSRL OP SD TP
2800 Powder Mill Road
Adelphi, MD 20783-1145

Director
Army Research Laboratory
AMSRL-CI-LP
Technical Library 305
APG, MD 21005-5066